Research Square

Preprints are preliminary reports that have not undergone peer review.
They should not be considered conclusive, used to inform clinical practice,
or referenced by the media as validated information.

Graphene-Enhanced Terahertz Metasurface Refractive-Index Sensor with an Ultrasmall Sensing Volume: A Numerical Study Relevant to Label-Free Biosensing

Aymen Bouali

aymen.bouali@ipest.u-carthage.tn

University of Tunis El Manar

Research Article

Keywords: terahertz metasurface, graphene, refractive-index sensing, label-free biosensing, single-cell-scale sensing, numerical study

Posted Date: May 6th, 2026

DOI: https://doi.org/10.21203/rs.3.rs-9458244/v1

License: This work is licensed under a Creative Commons Attribution 4.0 International License.
Read Full License

Additional Declarations: No competing interests reported.

Abstract

We numerically investigate a graphene-enhanced terahertz (THz) metasurface refractive-index sensor intended for label-free micro-volume biosensing and relevant to cancer-related refractive-index screening. The device consists of a gold split-gap resonator array operating near 1.6 THz, with a monolayer graphene patch inserted into the capacitive gap and covered by a thin analyte layer. The effective sensing volume is approximately 10 μm³, comparable to a single mammalian cell. Within the author-provided CST frequency-domain study, the bare metallic metasurface exhibits a refractive-index sensitivity of about 0.30 THz/RIU, whereas the graphene-loaded configuration reaches about 1.0 THz/RIU while preserving a comparable resonance linewidth. Fine-step numerical sweeps indicate an estimated refractive-index resolution better than 10^{-3} RIU. To keep the benchmarking defensible, the literature comparison is restricted to primary THz studies that explicitly report frequency sensitivity in GHz/RIU or THz/RIU; under this criterion, the proposed design remains competitive while operating in an ultrasmall sensing region. Because the present work is numerical and uses a simplified dielectric analyte model, it is positioned as a device-level proof of concept rather than a biological validation study.

1. Introduction

Label-free optical sensing is widely investigated for cancer-related screening because it probes intrinsic physical properties of cells and biofluids without relying on fluorescent or radioactive labels [1,2]. A recurring idea in that literature is that malignant transformation is often accompanied by small but measurable changes in refractive index, which makes refractive-index sensing a relevant device-level route for early discrimination studies [2].

In parallel, terahertz biosensing has attracted sustained interest because THz waves are non-ionizing, interact with low-frequency collective modes, and can convert local dielectric perturbations into measurable spectral signatures [3–8]. Recent reviews have highlighted the rapid development of THz metamaterial and metasurface sensors for label-free detection, especially when field localization is concentrated into subwavelength hotspots [4–8].

Graphene is particularly attractive in this context because its tunable surface conductivity and strong plasmonic response can increase near-field confinement in the THz regime [9–11]. Graphene-assisted THz sensing has therefore emerged as an active subfield in which metasurfaces are engineered to strengthen analyte–field overlap and improve refractive-index sensitivity [10,11].

A key conceptual precedent is the micro-gap THz metamaterial work of Park et al. [3], where biological objects comparable to the gap dimensions produced measurable resonance shifts. More recent studies have extended THz metasurface sensing to galactose films [12], apoptotic cells [13], breast-cell discrimination with graphene [14], polarization-insensitive cancer-cell sensing [15], amino-acid detection [16], biomolecular fingerprinting using all-dielectric metasurfaces [17], quasi-bound-state engineering [18], amino-acid solutions [19], cyanobacterial films [20], and pancreatic biomarkers [21].

The present manuscript aims to make a careful and submission-ready contribution within that landscape. The device is treated as a numerical proof of concept for an ultrasmall-volume THz refractive-index sensor. The biomedical framing is kept deliberately conservative: the platform is relevant to label-free cancer-related screening because the targeted refractive-index window overlaps the values reported for normal and cancerous cells [2], but no biological validation experiment is claimed here.

The main contributions are the following. First, the sensing region is confined to approximately 5 μm × 0.5 μm × 4 μm, i.e., about 10 μm³. Second, a graphene patch is inserted only in the capacitive gap to maximize field–analyte overlap. Third, the comparison with the literature is restricted to externally verifiable THz papers that explicitly report frequency sensitivity, avoiding unsafe conversions or inferred values.

2. Physical Basis and Numerical Model

2.1. LC perturbation picture

A periodic metallic THz metasurface can be interpreted, to first order, as an effective LC resonator. In this approximation, the resonance frequency is

$f_0 = 1 / (2\pi\sqrt{(LC_{eff})})$ (1)

When the gap region is filled with an analyte of refractive index n, the effective capacitance increases and the resonance red-shifts. In the perturbative limit, the response can be expressed as

$\Delta f_0 / f_0 \approx -(1/2)\, \eta\, (\Delta\varepsilon / \varepsilon_{eff})$ (2)

where η denotes the confinement factor between the resonant mode and the analyte. Increasing η is therefore a direct route to higher refractive-index sensitivity. The frequency sensitivity is written as

$S = \Delta f_0 / \Delta n$ (3)

2.2. Graphene response in the THz range

For monolayer graphene in the THz band, the intraband contribution of the Kubo formalism yields a Drude-like surface conductivity [9,10]:

$\sigma(\omega) \approx (e^2 / \pi\hbar^2)\, i\mu_c /(\omega + i\Gamma)$ (4)

Here μ_c is the chemical potential and Γ is the carrier scattering rate. A graphene patch placed inside the capacitive gap modifies the local boundary condition and can intensify the electric field at the graphene–dielectric interface [9–11]. Restricting the graphene to the gap region maximizes the overlap between the field hotspot and the analyte pocket.

2.3. Geometry and simulation settings

The unit cell consists of a pair of gold resonators patterned on a high-resistivity silicon substrate. The central gap is approximately 0.5 μm wide and 5 μm long, and it is covered by an analyte layer about 4 μm thick. The resulting effective sensing volume is therefore about 10 μm³.

The analyte is modeled as a non-absorbing dielectric characterized by a real refractive index in the range n = 1.33–1.41. This simplified model is suitable for a first device study, but it does not capture dispersion, absorption, heterogeneity, or cell morphology.

Graphene is represented as a monolayer surface with complex conductivity given by Eq. (4), implemented through a surface-impedance boundary condition. Representative parameters consistent with moderately doped graphene are used, with μ_c in the 0.3–0.5 eV range and a scattering rate of a few THz [9,10].

Electromagnetic simulations were carried out in CST Studio Suite using the frequency-domain solver. Periodic boundary conditions were applied along x and y, and open boundaries were used along z. The excitation is a normally incident plane wave polarized along the gap direction. A locally refined hexahedral mesh was employed in the gap and graphene region, with a minimum cell size below about 50–80 nm. The simulation band spans 1.55–1.67 THz with a frequency step of 1–2 GHz.

For each analyte refractive index, the transmission coefficient S21(f) was extracted and the resonance frequency was determined from the transmission minimum. The refractive-index sensitivity was obtained from the slope of a linear fit of resonance frequency versus refractive index.

3. Results

3.1. Bare metasurface response

The bare metallic metasurface exhibits a single resonance near 1.63 THz, and the resonance frequency decreases approximately linearly as the analyte refractive index increases. The extracted slope corresponds to a sensitivity of about 0.30 THz/RIU (approximately 300 GHz/RIU). In practical terms, an index change of 0.01 RIU produces a frequency shift of roughly 3 GHz.

3.2. Graphene-enhanced field localization

When the graphene patch is inserted into the gap, the electric field at resonance becomes markedly more localized inside the analyte pocket and along the graphene–metal interface. This is the central physical mechanism behind the performance improvement claimed for the graphene-loaded design: the mode overlap with the analyte is increased while the interaction region remains highly localized.

The field map retained in Fig. 4 is consistent with the intended device operation and supports the interpretation that graphene enhances the gap hotspot. For a refractive-index sensor, this stronger

confinement is advantageous because a fixed dielectric perturbation is translated into a larger spectral shift when the field energy is concentrated in the perturbed region.

3.3. Summary of extracted performance metrics

The key numerical outcomes of the author-provided CST study are summarized in Table 1. The graphene-loaded configuration is reported to increase the refractive-index sensitivity by approximately a factor of 3.3 relative to the bare-metal case, while maintaining an estimated refractive-index resolution better than 10^{-3} RIU. These values define the central performance claim of the manuscript and are therefore presented transparently as the internal metrics of the present numerical study.

Table 1
Internal summary of the numerical metrics reported for the present design.

Configuration	Resonance behavior	Sensitivity	Comment
Bare gold metasurface	Single dip near 1.63 THz	≈ 0.30 THz/RIU (≈ 300 GHz/RIU)	Frequency shift ≈ 3 GHz for Δn = 0.01
Graphene-loaded metasurface	Enhanced gap hotspot in the analyte pocket	≈ 1.0 THz/RIU (≈ 1000 GHz/RIU)	≈ 3.3× improvement relative to bare case
Fine RI sweep around operating point	Incremental spectral shift remains distinguishable	Estimated resolution better than 10^{-3} RIU	Simulation-based estimate within the present CST study

3.4. Reliable comparison with published THz studies

To keep the external benchmark defensible, Table 2 includes only primary THz studies that explicitly report frequency sensitivity in GHz/RIU or THz/RIU in the source itself. No conversion from nm/RIU is used, and no sensing volume is inferred from geometry when it is not explicitly reported. Under that conservative criterion, the present design remains competitive with recent THz metasurface biosensors, especially in terms of the predicted sensitivity level combined with a very small active sensing region.

The comparison also shows why cautious positioning is important. Some published studies emphasize large-area or ensemble sensing, some focus on biomolecular fingerprints rather than refractive-index sweeps, and others combine numerical and experimental validation [12–21]. The present manuscript is therefore positioned as a numerical device study that targets ultrasmall-volume refractive-index sensing, rather than as an experimentally validated cancer-diagnostic platform. Recent Optical and Quantum Electronics articles also illustrate the growing activity around THz metasurface biosensing in related architectures, including a graphene/gold/silver metasurface reporting 571 GHz/RIU and a hybrid MXene/black phosphorus/graphene metasurface reporting 1000 GHz/RIU [22,23].

Table 2
External benchmark restricted to primary THz studies that explicitly report frequency sensitivity in GHz/RIU or THz/RIU. No nm/RIU conversion and no inferred sensing-volume values are used.

Ref.	Platform	Application / analyte	Explicit frequency sensitivity	Study type
This work	Graphene-enhanced split-gap THz metasurface	Cancer-related RI screening	≈ 1000 GHz/RIU	Numerical
[12]	Free-standing complementary asymmetric metasurface	Galactose film	91.7 GHz/RIU	Experiment + simulation
[14]	Graphene metasurface with dual resonance	Breast cells	1.21 THz/RIU (1210 GHz/RIU)	Numerical
[15]	Polarization-insensitive THz metasurface biosensor	Cancer cell lines	504 GHz/RIU	Experiment + simulation
[16]	Graphene disk metasurface	Amino acids	333.33 GHz/RIU	Numerical
[19]	Asymmetrically folded dual-aperture ring metasurface	L-valine / L-phenylalanine solutions	370 GHz/RIU	Experiment + simulation
[21]	Toroidal THz metasensing platform	Pancreatic biomarkers	97.6 GHz/RIU	Simulation + bioassay
[22]	Graphene/Au/Ag THz metasurface biosensor	Salinity	571 GHz/RIU	Numerical + ML
[23]	Hybrid MXene/BP/graphene THz metasurface biosensor	Pregnancy detection	1000 GHz/RIU	Numerical

4. Discussion and Practical Limitations

The main strength of the present design is the combination of two features that are not often achieved together in simple THz resonators: a high predicted frequency sensitivity and an ultrasmall active sensing region. That combination is attractive for localized probing, low sample consumption, and future integration with microfluidic confinement or optical cell positioning.

At the same time, the practical limitations must be stated explicitly. First, the study is purely numerical. Second, the analyte is represented as a homogeneous lossless dielectric, whereas real cells and biofluids are dispersive, lossy, heterogeneous, and often water-rich. Third, the fabrication of a 0.5 μm gap with a localized graphene patch requires tight lithographic alignment and realistic consideration of graphene quality, contamination, and contact resistance. Fourth, experimental frequency resolution, thermal drift, and sample-placement variability are not yet quantified.

These limitations do not invalidate the device concept, but they define the next steps required for publication-grade experimental translation: (i) fabrication with reproducible graphene transfer or direct growth, (ii) measurements on calibrated liquids and polymer films, (iii) tolerance studies for gap width and graphene parameters, and (iv) finally, biological tests on controlled cell samples or biomarker solutions.

Within that honest scope, the manuscript contributes a cleaner comparison framework than the initial draft. The benchmark now relies only on verifiable THz-frequency sensitivities from primary sources [12,14–16,19,21–23], while the broader discussion is supported by recent reviews and related THz metasurface papers [4–11,17,18,20].

5. Conclusion

We have presented a revised numerical study of a graphene-enhanced THz metasurface refractive-index sensor with an effective sensing volume of approximately 10 μm^3. Within the underlying CST study, the predicted sensitivity increases from about 0.30 THz/RIU for the bare metallic resonator to about 1.0 THz/RIU when graphene is inserted into the split gap.

The manuscript is intentionally positioned as a device-level proof of concept. It does not claim biological validation, but it does show that a graphene-assisted THz hotspot can plausibly support high-sensitivity, ultrasmall-volume refractive-index sensing relevant to label-free biosensing.

A conservative external comparison based only on explicit THz frequency-sensitivity values indicates that the proposed design is competitive with recent THz metasurface studies. The most important future step is experimental validation under realistic material and fluidic conditions.

Declarations

Conflict of interest.

The author declares no known competing financial interests or personal relationships that could have influenced the work reported in this manuscript.

Data and software. Electromagnetic simulations were carried out in CST Studio Suite. Raw CST project files and exported spectral data should be archived before submission to support reproducibility and reviewer queries.

Author Contribution

A.B. conceived the study, designed the metasurface, performed the numerical simulations, analyzed the data, and wrote and revised the manuscript.

Data Availability

The data supporting the findings of this study are generated from numerical simulations performed using CST Studio Suite. The simulation files and extracted datasets are available from the corresponding author upon reasonable request.

References

1. B. Kaur, S. Kumar, B.K. Kaushik, “Recent advancements in optical biosensors for cancer detection,” Biosens. Bioelectron. 197, 113805 (2022). https://doi.org/10.1016/j.bios.2021.113805.
2. T. Parvin, K. Ahmed, A.M. Alatwi, A.N.Z. Rashed, “Differential optical absorption spectroscopy-based refractive index sensor for cancer cell detection,” Opt. Rev. 28, 134–143 (2021). https://doi.org/10.1007/s10043-021-00644-w.
3. S.J. Park, J.T. Hong, S.J. Choi et al., “Detection of microorganisms using terahertz metamaterials,” Sci. Rep. 4, 4988 (2014). https://doi.org/10.1038/srep04988.
4. Y. Roh, T. Kim, G. Lee, M. Seo, E.-S. Yu, “Advances in terahertz biosensors toward photon-molecule interplay,” TrAC Trends Anal. Chem. 175, 117715 (2024). https://doi.org/10.1016/j.trac.2024.117715.
5. W. Zhang, J. Lin, Z. Yuan et al., “Terahertz Metamaterials for Biosensing Applications: A Review,” Biosensors 14, 3 (2024). https://doi.org/10.3390/bios14010003.
6. Z. Zhang, R. Zhao, M. Cong, J. Qiu, “Developments of terahertz metasurface biosensors: A literature review,” Nanotechnol. Rev. 13, 202300182 (2024). https://doi.org/10.1515/ntrev-2023-0182.
7. W. Wang, K. Sun, Y. Xue et al., “A review of terahertz metamaterial sensors and their applications,” Opt. Commun. 556, 130266 (2024). https://doi.org/10.1016/j.optcom.2024.130266.
8. Q. Wang, Y. Chen, J. Mao, F. Yang, N. Wang, “Metasurface-Assisted Terahertz Sensing,” Sensors 23, 5902 (2023). https://doi.org/10.3390/s23135902.
9. T. Low, P. Avouris, “Graphene plasmonics for terahertz to mid-infrared applications,” ACS Nano 8, 1086–1101 (2014). https://doi.org/10.1021/nn406627u.
10. S. Ogawa, S. Fukushima, M. Shimatani, “Graphene Plasmonics in Sensor Applications: A Review,” Sensors 20, 3563 (2020). https://doi.org/10.3390/s20123563.
11. H. Bi, M. Yang, R. You, “Advances in terahertz metasurface graphene for biosensing and application,” Discover Nano 18, 63 (2023). https://doi.org/10.1186/s11671-023-03814-8.
12. F. Taleb, I. Al-Naib, M. Koch, “Free-Standing Complementary Asymmetric Metasurface for Terahertz Sensing Applications,” Sensors 20, 2265 (2020). https://doi.org/10.3390/s20082265.
13. C. Zhang, L. Liang, L. Ding et al., “Label-free measurements on cell apoptosis using a terahertz metamaterial-based biosensor,” Appl. Phys. Lett. 108, 241105 (2016). https://doi.org/10.1063/1.4954015.

14. C. Tan, S. Wang, S. Li et al., “Cancer Diagnosis Using Terahertz-Graphene-Metasurface-Based Biosensor with Dual-Resonance Response,” Nanomaterials 12, 3889 (2022). https://doi.org/10.3390/nano12213889.
15. P. Wang, J. Lou, Y. Yu et al., “An ultra-sensitive metasurface biosensor for instant cancer detection based on terahertz spectra,” Nano Res. 16, 7304–7311 (2023). https://doi.org/10.1007/s12274-023-5386-7.
16. S.K. Patel, J. Surve, J. Parmar et al., “Terahertz Metasurface-Based Refractive Index Sensor for Amino Acid Detection: A Numerical Approach,” IEEE Trans. Nanobiosci. 22, 614–621 (2023). https://doi.org/10.1109/TNB.2022.3222446.
17. Q. Xu, M. Sun, W. Wang, Y. Shi, “All-Dielectric Metasurface-Based Terahertz Molecular Fingerprint Sensor for Trace Cinnamoylglycine Detection,” Biosensors 14, 440 (2024). https://doi.org/10.3390/bios14090440.
18. J. Peng, X. Lin, X. Yan et al., “Terahertz Biosensor Engineering Based on Quasi-BIC Metasurface with Ultrasensitive Detection,” Nanomaterials 14, 799 (2024). https://doi.org/10.3390/nano14090799.
19. J. Shu, X. Zhou, J. Hao et al., “Terahertz Sensing of L-Valine and L-Phenylalanine Solutions,” Sensors 24, 3798 (2024). https://doi.org/10.3390/s24123798.
20. T.H. Jeong, S.W. Jun, Y.H. Ahn, “Metamaterial Sensing of Cyanobacteria Using THz Thermal Curve Analysis,” Biosensors 14, 519 (2024). https://doi.org/10.3390/bios14110519.
21. P. Wang, M. Jiang, Q. Jia et al., “Early Pancreatic Cancer Diagnosis via Ultrasensitive THz Toroidal Metasensing,” Adv. Photonics Res. 6, 2500133 (2025). https://doi.org/10.1002/adpr.202500133.
22. J. Wekalao, N. Mandela, “Terahertz metasurface biosensor for high-sensitivity salinity detection and data encoding with machine learning optimization based on random forest regression,” Opt. Quant. Electron. 56, 1826 (2024). https://doi.org/10.1007/s11082-024-07777-7.
23. J. Wekalao, O. Elamri, “Novel terahertz biosensor integrating MXene/black phosphorus/graphene on metasurface architecture for enhanced pregnancy detection,” Opt. Quant. Electron. 57, 261 (2025). https://doi.org/10.1007/s11082-025-08205-0.

Figures

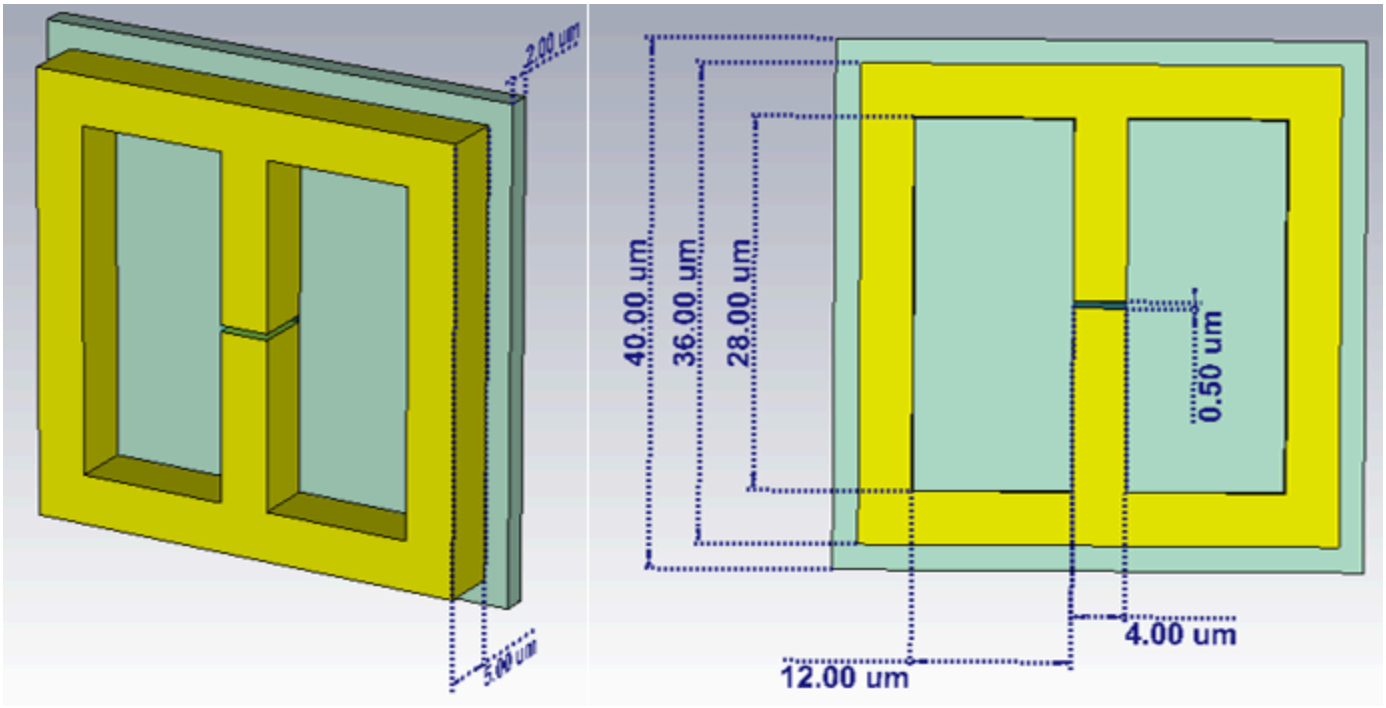


Figure 1

3D view (left) and top view (right) of the unit cell. The central split gap defines the main sensing region.

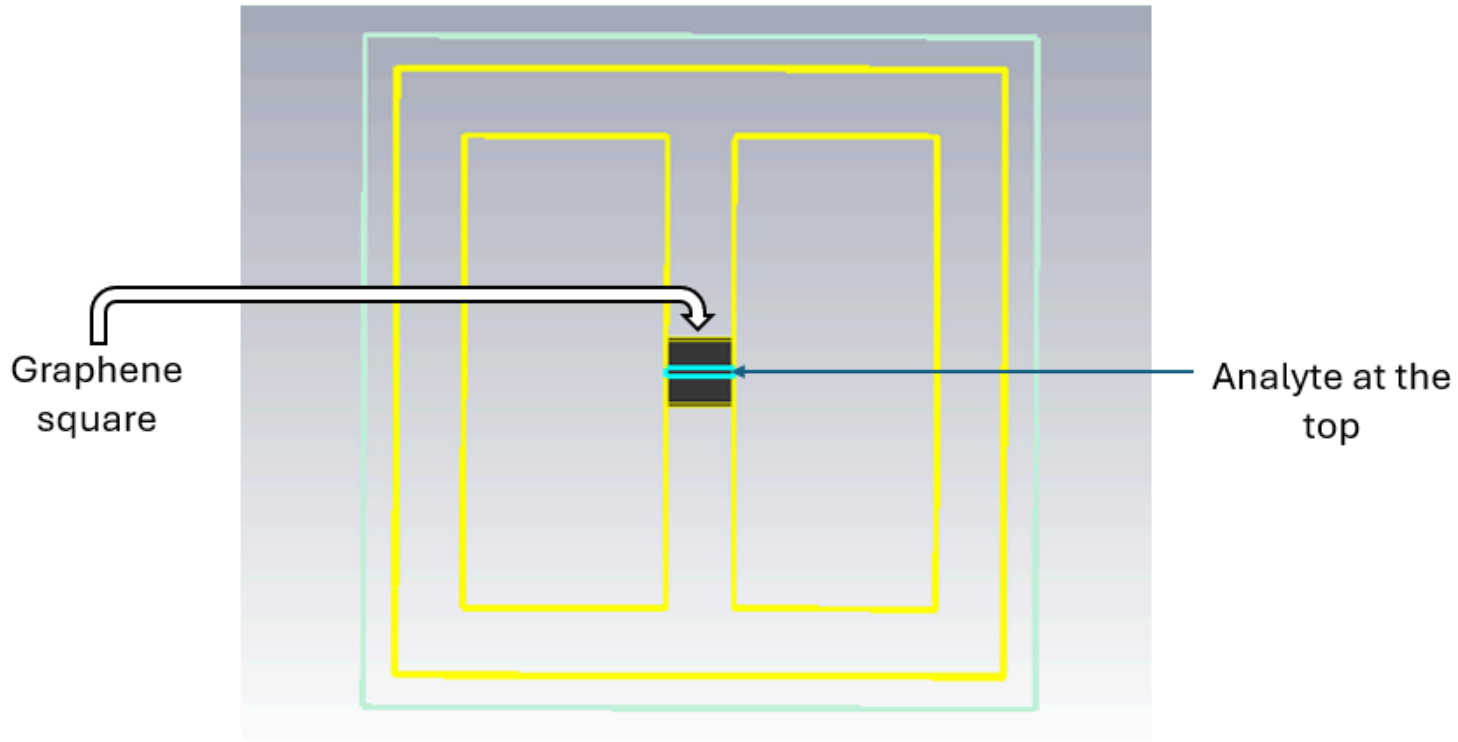


Figure 2

Top view of the graphene patch placed in the central gap and covered by the analyte layer.

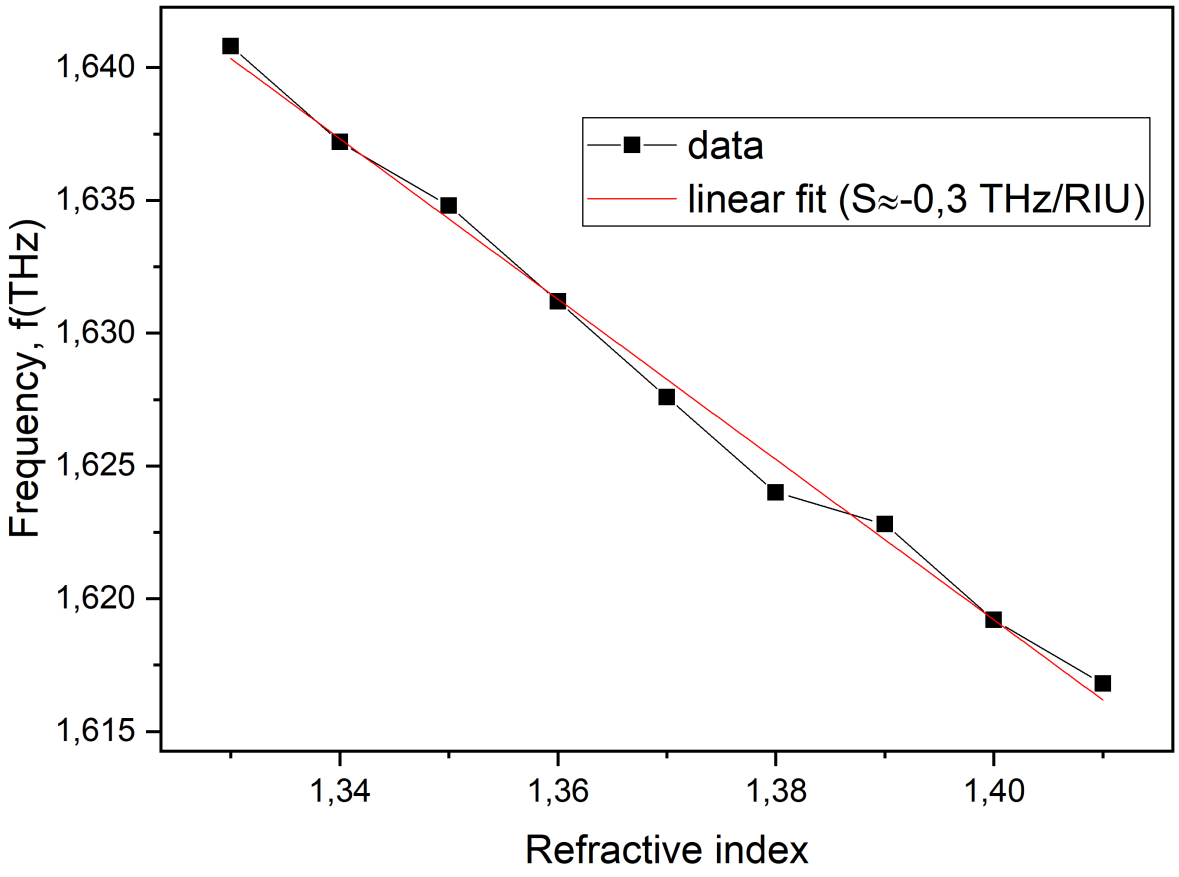


Figure 3

Bare-metasurface resonance frequency as a function of analyte refractive index. The linear trend yields a sensitivity of about 0.30 THz/RIU.

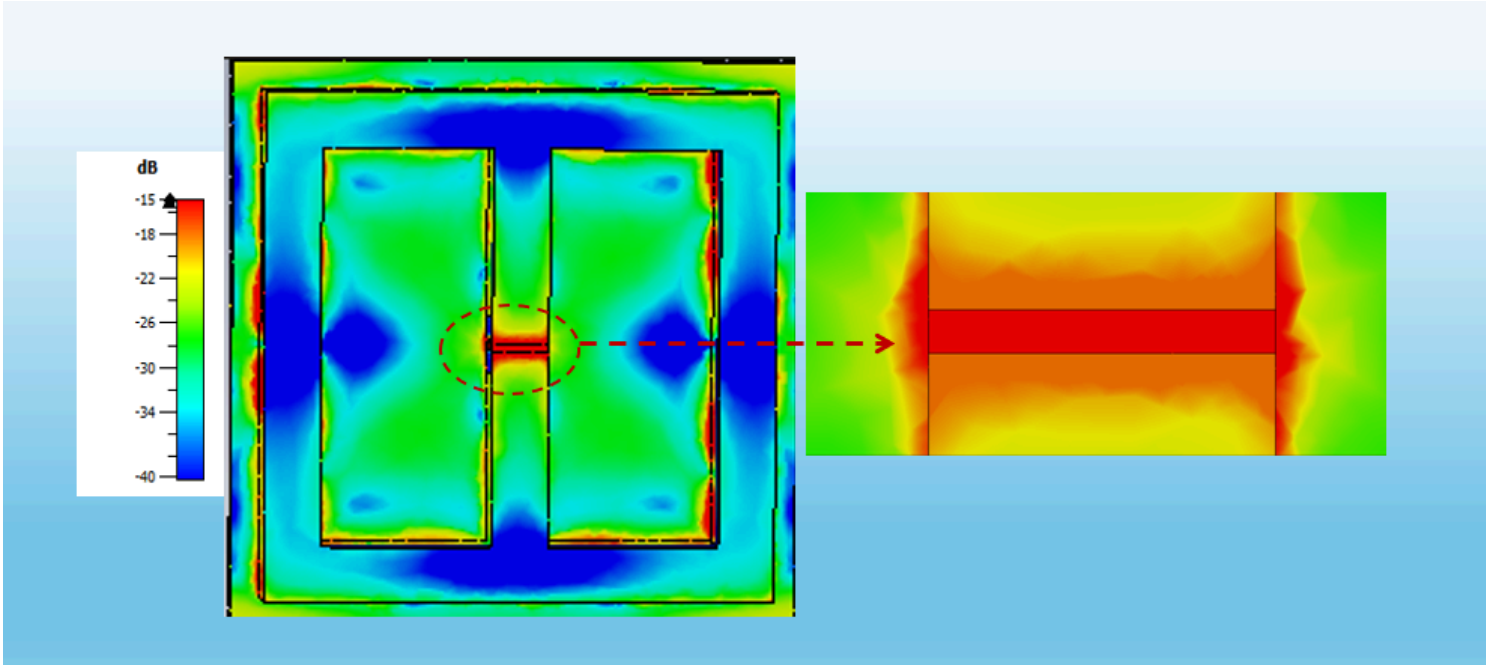


Figure 4

Simulated electric-field distribution at resonance for the graphene-loaded configuration. The hotspot is concentrated inside the central gap and analyte pocket.